Robust Wireless Power and Data Transmission System against Misalignment for Implantable Medical Devices

Haoqi Zhu, *Member, IEEE*, Xu Wu, *Member, IEEE*, Feng Xiong, and Mustafa Tahir, *Member, IEEE*

***Abstract*—Implantable medical devices with wireless power and data transmission (WPDT) are rapidly developing. However, they suffer from performance degradation issues due to misalignment between transmitter and receiver coils. To improve the system's robustness against misalignment, this article develops an innovative WPDT circuit incorporating an impedance matching network (IMN) in a Class-E power amplifier (PA). First, the target impedance region is identified to obtain the high-efficiency power transmission of the Class-E PA. Then, an ASK modulation scheme is implemented using MOSFETs and a data modulation inductor to transmit data. Leveraging the theoretical derivations about the target impedance region, the IMN circuit is implemented to keep impedance within the target region, avoiding performance degradation due to misalignment. Finally, the robustness proposed WPDT with an IMN circuit is validated through experiments for 10 mm misalignment, demonstrating a 17% improvement in efficiency compared with a conventional WPDT system without an IMN circuit. The experiment also validates that the bit error bit, which evaluates the data transmission reliability, remains less than 10^{-6} for a 1-Mbps data rate with a modulation index of 10%.**

***Index Terms*—Class-e power amplifier (PA), impedance matching network (IMN), implantable medical devices (IMDs), wireless power and data transmission (WPDT).**

I. Introduction

WIRELESS power and data transmission (WPDT) have been extensively researched in implantable medical devices (IMDs), such as cochlear implants [1], deep brain stimulator [2], etc., for the diagnosis and treatment of organ dysfunction, as depicted in Fig. 1. The power transmission requirements for IMDs can vary significantly, spanning from microwatt levels to several hundred milliwatts, contingent upon the specific application and its operational demands [3]. The data rate requirements also vary based on the application (e.g., retinal prostheses: 2–20 Mbps, cochlear implants: 1 Mbps) [4]. High power transmission efficiency and data transmission reliability are imperative to extend battery life and enable real-time monitoring, especially in cases of coil misalignment.

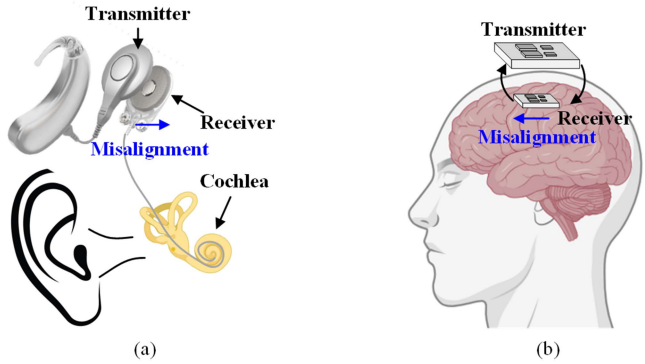

Fig. 1. Implantable medical devices. (a) Cochlear implant. (b) Deep brain stimulator.

For the WPDT system, robustness is crucial to withstand variations in the coil's relative position. The full-bridge converter is commonly used in WPDT of low-frequency and high-power situations because it is insensitive to load variation [5]. However, its square-waveform operation results in high total harmonic output voltage distortion. This disadvantage significantly affects the electromagnetic interference characteristic of the MHz WPDT system. Besides, operating an MHz system with a full-bridge converter poses challenges due to dead-time requirements [5].

For the MHz WPDT system in IMDs, the Class-E power amplifier (PA) is a promising candidate to drive high-frequency inductive links, thanks to its zero-voltage switching (ZVS) characteristics and zero-voltage-derivative switching (ZVDS) [6]. Although the PA has a high-efficiency characteristic, it is highly sensitive to variations in the load. When its load parameters deviate from their optimal value, the system's efficiency degrades [7]. Besides, the voltage amplitude also gets changed. Consequently, utilizing the characteristic of voltage amplitude change, the amplitude shift keying (ASK) modulation scheme, known for its lower power consumption and simpler structure design, is commonly utilized for data transmission [8], [9].

In the IMDs, the receiver coil is placed inside the body, while the transmitter coil is located outside to transmit power and

Received 11 February 2025; revised 23 April 2025; accepted 19 May 2025. Date of publication 23 May 2025; date of current version 30 June 2025. Recommended for publication by Associate Editor O. Lucia. *(Corresponding author: Haoqi Zhu.)*

Haoqi Zhu and Mustafa Tahir are with the College of Electrical Engineering, Zhejiang University, Hangzhou 310027, China, and also with Shaoxing Institute, Zhejiang University, Shaoxing 312099, China (e-mail: hqzhu23@zju.edu.cn; mustafatahir@zju.edu.cn).

Xu Wu is with NARI Group Corporation, Nanjing 210003, China (e-mail: wuxu0922@zju.edu.cn).

Feng Xiong is with College of Physica and Electronic Science, Hubei Normal University, Huangshi 435002, China (e-mail: xf1207@stu.hbnu.edu.cn).

Color versions of one or more figures in this article are available at https://doi.org/10.1109/TPEL.2025.3572948.

Digital Object Identifier 10.1109/TPEL.2025.3572948

data. Continuous body movement makes it difficult to ensure proper alignment between the receiver and transmitter coils [10], making it possible to have a wide range of mutual inductance variations between coils. This phenomenon leads to a wide range of coupling coefficient and load characteristic variations, thereby degrading the system's power transmission efficiency [11]. Furthermore, the modulation index (MI) of data transmission is affected by mutual inductance variations, resulting in an increased BER and decreased data transmission reliability [12]. Therefore, coil misalignment emerges as a fundamental challenge in WPDT systems for IMDs, directly hindering the achievement of high-efficiency transmission and reliable data transmission—both of which are essential for the safe and reliable operation of implantable devices.

To address this issue, researchers have explored innovative solutions to enhance the system's robustness against misalignment between coils. One commonly employed approach involves optimizing the geometry structures of the coils or adopting multicoil strategies [13]. By carefully designing and adjusting the shape and size of the coils, it is possible to improve their alignment and ensure stable power transmission efficiency. In [14], a 3-D receiver and transmitter coil model is presented to tackle the issue of misalignment sensitivity. In addition, a sphere-shaped receiver coil is reported in [15] to impair the impact of misalignment between coils. Furthermore, enlarging the size of both the transmitter and receiver coil is proposed as a means to improve misalignment tolerance [16], [17]. Ke et al. [18] propose a multicoil receiver to enhance the misalignment tolerance. A dual-resonant mixed-coupling coil is also reported in [19] to enhance the misalignment immunity. Although these methods mentioned above can effectively improve robustness against misalignment in wireless power transmission (WPT), they are not suitable for IMD applications due to stringent size requirements.

Among control-oriented solutions, a self-oscillation control strategy is presented in [20] and [21] to ensure a pure resistance input impedance, which effectively mitigates the system's output fluctuations caused by changes in the coupling coefficient due to coil misalignment. However, achieving accurate current/voltage sensing poses a challenge in the application of IMDs due to their operating frequency exceeding megahertz [22]. As an alternative method, a dynamic tuning control approach has been developed in [23], [24], and [25]. This method aims to adjust the resonance inductance and capacitance to maintain high efficiency and stable output characteristics when the coil is misaligned. However, it introduces additional passive components and switching devices to ensure a stable tuning state, resulting in increased system cost, volume, and complexity [26].

Alternatively, the impedance matching network (IMN) or compensation network methods are popular solutions for MHz WPT [27]. In [28], a Π-network consisting of some passive components is introduced into the WPT system to enhance the system's efficiency and stabilize output characteristics. A double-sided *LCC* compensation strategy is employed in [29] to provide constant output voltage and current over the coupling coefficient's variation caused by coil misalignment.

Nevertheless, despite the numerous reported studies on WPT, there is a lack of studies on WPDT that utilize the characteristics of IMN to improve both power and data transmission against misalignment ability. This is particularly important for IMDs, requiring highly reliable data transmission, high power transmission efficiency, and compact size.

Therefore, the motivation of this article is to address the challenges associated with achieving not only high power transmission efficiency but also data transmission reliability for IMDs in case of coil misalignment. The article presents an innovative WPDT circuit incorporating IMN to improve the robustness against misalignment. By incorporating an IMN circuit, the impedance transformation can be appropriately achieved, ensuring that the impedance meets the Class-E PA's target impedance region within the coupling coefficient range. A data modulation circuit is designed to integrate an inductor and MOSFETs into the Class-E PA, enabling simultaneous data transmission while maintaining high power transmission efficiency. A high data rate is achieved by applying a constraint condition on the data transmission rate in IMN circuit design. Notable contributions in this article include the following.

1) An innovative WPDT with an IMN circuit is developed to achieve high power transmission efficiency and reliable data transmission in case of coil misalignment, which improves the robustness against coil misalignment.
2) A unique constraint condition is implemented in the IMN circuit's design, enabling the calculation of IMN circuit parameters and achieving the desirable high data rates.
3) A misalignment weight factor is presented to indicate the significance of coil misalignment in relation to its vertical distance. By incorporating this weight factor, researchers can better quantify and evaluate the severity of coil misalignment.

The rest this article is organized as follows. The target impedance region for achieving the WPDT system's high-efficiency transmission is derived and discussed in Section II. Based on the target impedance region, a WPDT with an IMN circuit is demonstrated in Section III, including its analysis, calculation, and design procedure. In Section IV, a prototype is implemented to validate the proposed circuit's effectiveness. Finally, Section V concludes this article.

II. Working Principle of WPDT System

Class-E PA is frequently utilized in WPDT systems to drive the magnetic coupling resonance links, owing to its capability to achieve nearly 100% efficiency. However, Class-E demonstrates a high susceptibility to load variation, potentially causing a deterioration in efficiency performance. In WPDT, horizontal misalignment between the transmitter and receiver coils can alter the links' coupling coefficient, resulting in load impedance feature variations within the PA that diminish the efficiency. Therefore, it is essential to investigate the impedance range of the load to achieve high-efficiency transmission.

A. Equivalent Circuit Derivation for WPT

The schematic of the WPT is depicted in Fig. 2, showcasing the Class-E PA, series-parallel compensation capacitors, and coupling coils. In this diagram, L_r and L_t denote the receiver and transmitter coils, respectively, while r_t stands for the transmitter

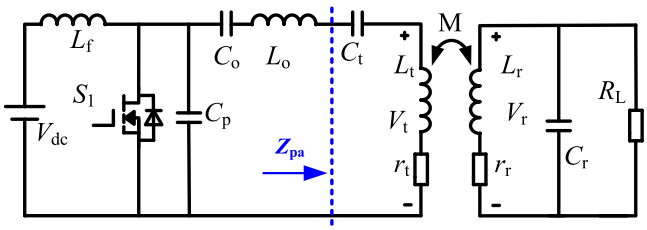

Fig. 2. WPT schematic.

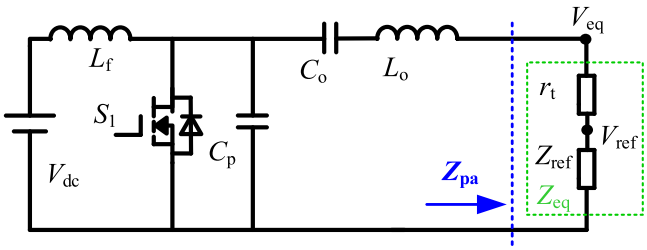

Fig. 3. Simplify the circuit model of WPT.

coil's equivalent series resistance (ESR), r_r is the receiver coil's ESR, C_r and C_t represent the parallel and series compensated capacitors. L_f indicates the choke inductor. C_o and L_o acts as the resonance capacitor and inductor, S_1 denotes the switching device, and C_p represents the shunt capacitor. R_L is the ac load.

In WPT systems, the receiver circuit is usually jointly with the transmitter circuit to facilitate the theoretical analysis and calculation. Consequently, Fig. 3 represents a simplified schematic of the WPT circuit seen in Fig. 2. In addition, ensuring that both the transmitter and receiver coils work at their resonant frequency (f_r) to optimize the power transmission efficiency is essential. Hence, f_r can be determined as follows:

$$f_r = \frac{1}{2\pi\sqrt{L_t C_t}} = \frac{1}{2\pi\sqrt{L_r C_r}}. \tag{1}$$

When the WPT systems operating frequency is equal to f_r, the reflected impedance Z_{ref} is calculated as follows:

$$\begin{cases} Z_{\text{ref}} = \frac{Q_r^2 r_r \times R_L}{n^2(Q_r^2 r_r + R_L)} = \frac{k^2\omega_r^2 L_t L_r R_L}{R_L r_r + \omega_r^2 L_r^2} \\ Z_{\text{eq}} = Z_{\text{ref}} + r_t \end{cases} \tag{2}$$

where Q_r is the receiver coil's quality factor, its expression denotes $\omega_r L_r/r_r$, and $\omega_r = 2\pi f_r$. k represents the coupling coefficient between coils, and Z_{eq} denotes equivalent impedance.

According to (2), Z_{eq} is purely resistive, with its value mainly determined by k. In Fig. 3, Z_{eq} is identified as Class-E PA's load impedance Z_{pa} ($Z_{\text{pa}} = R_{\text{pa}} + jX_{\text{pa}}$). However, this PA demonstrates a high sensitivity to changes in its load impedance. As a result, coupling coefficient variations directly impact the PA's load impedance, which can significantly deteriorate its transmission efficiency.

B. Impedance Target Region for Class-E PA

To achieve maximum efficiency of the Class-E PA, it is crucial to satisfy both the ZVS and ZVDS, which requires a certain configuration value of the L_o-C_o-C_p-Z_{pa} network for matching.

TABLE I
CIRCUIT PARAMETERS

Parameters	Description	Value
f_s	Carrier frequency	16 MHz
V_{dc}	DC input voltage	3.3 V
C_p	Parallel capacitor	40 pF
C_o	Resonance capacitor	40 pF
L_o	Resonance inductor	3 μH
D	Duty cycle	0.5

Hence, in this state, the shunt capacitor and resonance capacitor are calculated as follows [28].

$$\begin{cases} C_p = \frac{8}{\pi(\pi^2+4)\omega_r R_{\text{pa}}} \\ C_o = \frac{16}{\omega_r R_{\text{pa}}[16Q_L - \pi(\pi^2+4)]} \end{cases} \tag{3}$$

where the Q_L indicates the Class-E PA's load quality factor, which is equal to $\omega_r L_o/R_{\text{pa}}$.

Based on the above-mentioned analysis, the optimal performance at a fixed load parameter can be guaranteed using the traditional design method for the Class-E PA, e.g., efficiency and output power. However, obtaining the impedance Z_{pa} target region for Class-E PA design is critical to achieving high-efficiency transmission characteristics when the coils are misaligned. The PA's operating condition must be known to investigate the target impedance range. In the WPDT system of IMDs, the output power is typically less than 100 mW [12]. Besides, the 16 MHz carrier frequency is employed to drive the Class-E PA. The values of the resonance inductance L_o and choke inductance L_f are selected as 3 and 2.7 μH, respectively. Following the requirements for optimal parameters design, C_p and C_o are set to 40 and 40 pF using (3). The Class-E PA's efficiency and output power are subsequently investigated. The details of the parameters are outlined in Table I.

Note that a 0.5 duty cycle is selected, and the PA's stray parameters are neglected in this study. Hence, the output power and efficiency are calculated following the equation provided as follows [30]:

$$\begin{cases} P_{\text{out}} = \frac{I_{\text{out}}^2}{R_{\text{eq}}} = I_{\text{out}} V_{\text{eq}} \\ \eta = \frac{P_{\text{out}}}{P_{\text{in}}} = \frac{P_{\text{out}}}{I_{\text{dc}}^2 R_{\text{dc}}} \end{cases} \tag{4}$$

where I_{out} and I_{dc} denote the PA's output and input currents, respectively, R_{dc} represents the PA's dc resistance, V_{eq} indicates the PA's output voltage, P_{in} and P_{out} are the PA's input and output power

$$\begin{cases} I_{\text{out}} = \frac{gV_{\text{dc}}}{R_{\text{dc}}}, I_{\text{dc}} = \frac{V_{\text{dc}}}{R_{\text{dc}}}, V_{\text{eq}} = \frac{gV_{\text{dc}}R_{\text{eq}}}{R_{\text{dc}}} \\ R_{\text{dc}} = \frac{\pi^2 + g[2\pi\sin(\phi - 0.5\pi) - 4\sin\phi]}{4\pi\omega_r C_s} \end{cases} \tag{5}$$

where g and ϕ denote the dc–ac voltage's transfer ratio and the load current phase, respectively. These can be determined

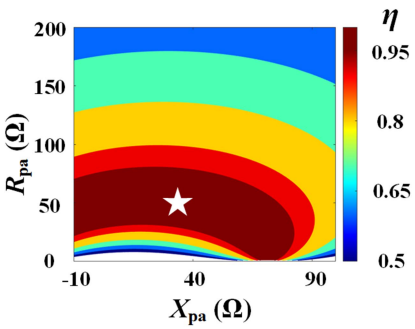

Fig. 4. Efficiency with different Z_{pa} ($Z_{pa} = R_{pa}+X_{pa}$).

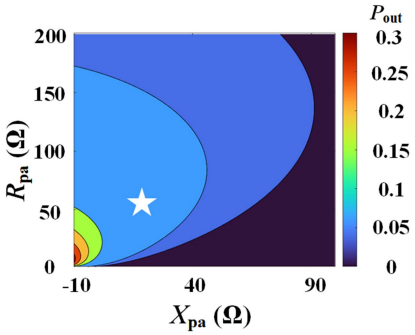

Fig. 5. Output power with different Z_{pa} ($Z_{pa} = R_{pa}+X_{pa}$).

through the following calculations

$$\begin{cases} g = \frac{\pi \sin(\phi+\varphi)+2\cos(\phi+\varphi)}{-2\sin(\phi-0.5\pi)\sin(\phi+\varphi)+0.5\pi\cos\varphi} \\ \phi = \arctan\left(-\frac{4-0.5\pi^2+(2\cos\varphi+\pi\sin\varphi)s}{\pi+(\pi\cos\varphi-2\sin\varphi)s}\right) \end{cases}. \tag{6}$$

The load phase φ and coefficient are defined as follows:

$$\begin{cases} \varphi = \arctan\left(\frac{\omega_r L_o-(\omega_o C_o)^{-1}+X_{pa}}{R_{pa}}\right) \\ s = \pi\omega_r C_s R_{pa}\sqrt{1+\tan^2\varphi} \end{cases}. \tag{7}$$

Utilizing (4)–(7), the impedance range ($Z_{pa} = R_{pa}+jX_{pa}$) is swept to obtain the high-efficiency and a suitable output power region. Fig. 4 demonstrates the efficiency curve's variation with regard to Z_{pa} ($Z_{pa} = R_{pa}+jX_{pa}$). It illustrates the contour map of efficiency, highlighting the region where η>0.95 with a star symbol. The Class-E PA's output power variation trend for different Z_{pa} is illustrated in Fig. 5, and the output power's contour map is displayed. Considering the circuit losses and the IMDs' output power requirement, an appropriate output power range for Class-E PA might be [0.05, 0.12]. The target region is marked with a star symbol in Fig. 5. Therefore, considering efficiency and output power requirements, the target impedance Z_{pa} range is defined as [−6, 40] for X_{pa} and [40, 67] for R_{pa}.

C. Data Modulation Implementation

Fig. 6 demonstrates the proposed data modulation circuit in this study. The presented circuit expands upon the framework depicted in Fig. 2 by incorporating data modulation, denoted by the purple. The data modulation circuit involves switching

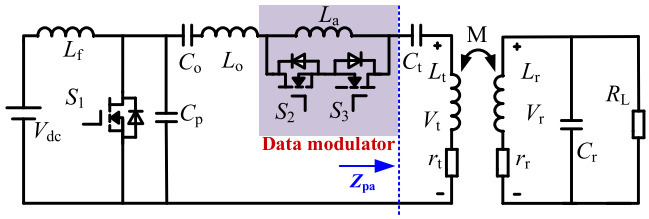

Fig. 6. WPDT circuit.

devices S_2, S_3, and inductor L_a. Its implementation process is demonstrated as follows.

The switching devices (S_2 and S_3) will turn ON when the data-signal is 1, allowing the Class-E PA to operate optimally tuned to achieve the highest efficiency transmission. Conversely, S_2 and S_3 will turn OFF when the data-signal is 0, and the PA's load network incorporates L_a. In this state, the load network's reactance increases, which reduces the transmitter coil's voltage amplitude. Thus, the ASK modulation method is implemented for the data-signal transmission. However, it is essential to note that there exists a trade-OFF between the bit error rate and power transmission efficiency when choosing the value of L_a. Reducing the L_a can increase efficiency, but it may also result in an increased bit error rate. Hence, designing the appropriate L_a value is critical for the proposed data modulation scheme.

As stated before, when the data-signal is 1, the Class-E PA operates optimally tuned. In this state, it is well known that the load phase φ is approximately 49°, and the efficiency is highest [31]. Furthermore, by substituting φ into (5) and (6) to obtain an empirical formula, the relationship between tan(φ) and the voltage amplitude of receiver voltage V_r can be expressed as follows:

$$V_r = \frac{1}{k}\sqrt{\frac{L_r}{L_t}}\left[1.83V_{dc}\exp(-0.47\tan\varphi)\right]. \tag{8}$$

For ASK modulation, the MI is directly related to the L_a, which impacts both efficiency and bit error rate, and its expression is defined by

$$\mathrm{MI} = \frac{V_{r\_H}-V_{r\_L}}{V_{r\_H}+V_{r\_L}}. \tag{9}$$

When the data-signal is 0 and 1, V_{r_L} and V_{r_H} represent the receiver coil's output voltage amplitudes, respectively. The expression of V_{r_H} is as

$$V_{r\_H} = \frac{1}{k}\sqrt{\frac{L_r}{L_t}}(1.07V_{dc}). \tag{10}$$

The Class-E PA incorporates L_a when the data-signal is 0. Combined with (7) and (8), V_{r_L} is expressed as follows:

$$V_{r\_L} = \frac{1}{k}\sqrt{\frac{L_r}{L_t}}\left[1.07V_{dc}\exp\left(\frac{-0.47\omega_r L_a}{R_{pa}}\right)\right]. \tag{11}$$

Substituting (10) and (11) into (9), the value of L_a is deduced as follows:

$$L_a = \frac{-R_{pa}}{0.47\omega_r}\ln\left(\frac{1-\mathrm{MI}}{1+\mathrm{MI}}\right). \tag{12}$$

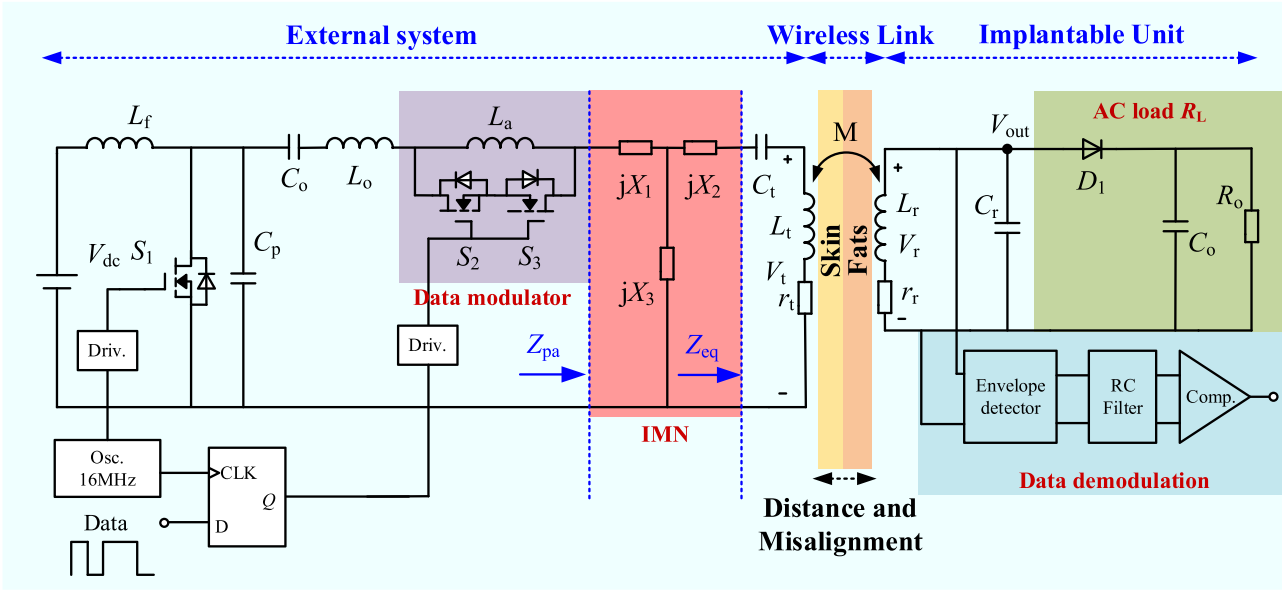

Fig. 7. Schematic of the proposed WPDT with an IMN circuit for IMDs.

Based on (12), the L_a is proportional to MI. A larger MI leads to lower efficiency, while the bit error rate is also lower. Hence, to enhance transmission efficiency, the MI is typically designed to be 0.1 [31].

III. Proposed WPDT With IMN Circuit

This section elucidates the proposed WPDT system with an IMN circuit to improve the system's robustness against misalignment.

Fig. 7 demonstrates the proposed WPDT with an IMN circuit in this study. The presented circuit expands upon the framework depicted in Fig. 6 by incorporating separate modules for IMN, data demodulation, and ac load R_L, denoted by the red, blue, and green boxes, respectively. Specifically, the data demodulation circuit comprises an RC filter, an envelope detector, and a comparator, which work in converting and extracting the data signal.

If the proposed circuit is configured without IMN, the Class-E PA's load impedance $Z_{\rm pa}$ is equal to the $Z_{\rm eq}$. As a result, the system's characteristics are determined by the $Z_{\rm eq}$, and both efficiency and output power are significantly dependent on the coupling coefficient k. By incorporating an IMN circuit, the impedance transformation for $Z_{\rm eq}$ can be appropriately achieved, ensuring that the impedance meets the Class-E PA's target impedance region within the range of k [28].

The cochlea implant is used as a demonstration application to validate the proposed concept. Utilizing the coil design criteria outlined in [32], a circular PCB-type coil, as shown in Fig. 8, is identified as an appropriate choice for WPDT. The design specifies the transmitter and receiver coils to have inductance values of 3 and 1 μH, respectively. At a frequency of 16 MHz, the ESR for the transmitter coil (r_t) and receiver coil (r_r) are measured to be 0.44 and 0.36 Ω, respectively. The specific dimensions of these coils are detailed in Table II.

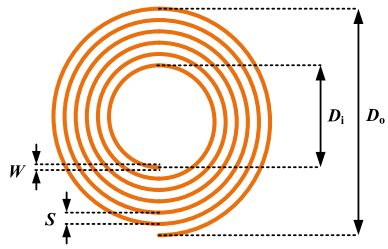

Fig. 8. Circular PCB-type coil's geometry structure.

TABLE II
Transmitter and Receiver Coil Dimensions

Parameters	Description	Transmitter coil/ Receiver coil
D_i	Inner diameter	22 mm/20 mm
D_o	Outer diameter	27.2 mm/23.6 mm
S	Turn spacing	0.12 mm/0.12 mm
W	Turn width	0.25 mm/0.25 mm
n	Coil turn number	8/5

For cochlear implant applications, the distance between the receiver and transmitter coils has been meticulously set to 5 mm, taking into account the body's fat layers and skin thickness [32], [33]. The misalignment distance of ±10 mm between coils is also considered to validate the system as a worst-case scenario [34], as illustrated in Fig. 9(a). ANSYS is utilized to evaluate the coils' coupling coefficient variation under these conditions. ANSYS provides designers with valuable insight into the interaction of electromagnetic fields. The result in Fig. 9(b) indicates that k ranges from 0.12 to 0.19 in the case of the coil misalignment distance of ±10 mm. In Fig. 9(b), experimental measurements are conducted to validate the simulation results' accuracy. As a

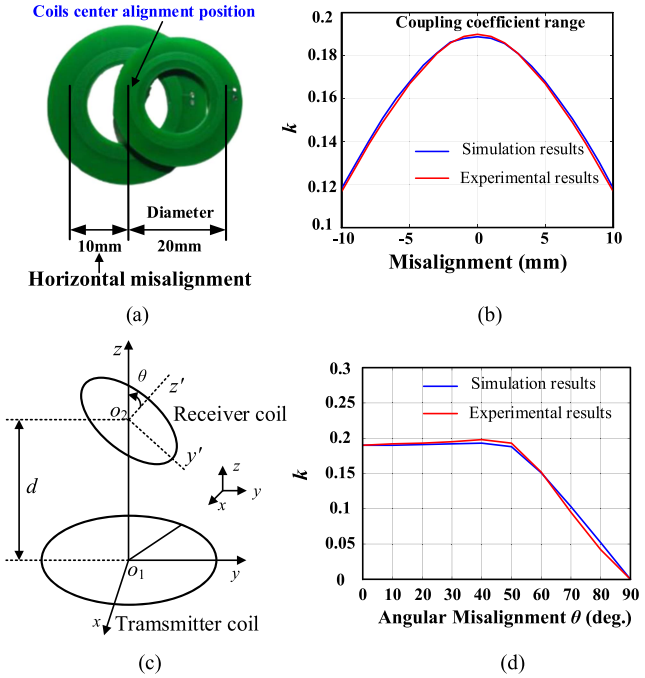

Fig. 9. Coupling coil misalignment. (a) Circular PCB-type coupling coils. (b) Coupling coefficient variation trend with coils misalignment distance. (c) Angular coil configuration. (d) Coupling coefficient variation trend with coils angular misalignment.

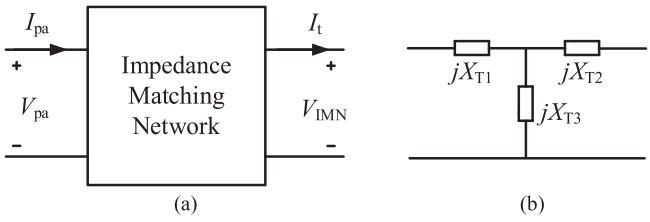

Fig. 10. IMN implementation. (a) Two-port network for IMN. (b) T-model.

result, the ANSYS simulation results closely match the experimental measurements, demonstrating its validity. Furthermore, the variation of the coupling coefficient in terms of angular misalignment is investigated from both the ANSYS simulations and experimental measurements. Fig. 9(c) depicts the angular coil configuration, while the coupling coefficient variation trend with coil angular misalignment is illustrated in Fig. 9(d). The coupling coefficient demonstrates a significant decline when the coil angular misalignment exceeds 50°. Notably, the coupling coefficient approaches zero when the coil angular misalignment reaches 90° (the worst-case scenario). For the coil angular misalignment, the experimental measurements validate the effectiveness of the simulation results.

On substituting k into (2), $R_{\rm pa}$ will deviate from the target region when k is less than 1.7. To ensure the impedance $Z_{\rm pa}$ remains within the target region, an IMN circuit is employed, as illustrated in Fig. 10. Fig. 10(a) shows the two-port of IMN, and its expression is represented as follows:

$$\begin{bmatrix} V_{\rm pa} \\ V_{\rm IMN} \end{bmatrix} = \begin{bmatrix} Z_{11} & Z_{12} \\ Z_{21} & Z_{22} \end{bmatrix} \begin{bmatrix} I_{\rm pa} \\ -I_t \end{bmatrix}. \tag{13}$$

Generally, the two-port network consists of passive components, (13) is simplified as follows:

$$\begin{bmatrix} V_{\rm pa} \\ V_{\rm IMN} \end{bmatrix} = \begin{bmatrix} jX_{11} & jX_{12} \\ jX_{21} & jX_{22} \end{bmatrix} \begin{bmatrix} I_{\rm pa} \\ -I_t \end{bmatrix}. \tag{14}$$

Combined with (2), $V_{\rm IMN}$ is equal to $Z_{\rm eq}I_t$. Hence, $Z_{\rm pa}$ can be obtained by

$$Z_{\rm pa} = jX_{11} + \frac{X_{12}^2}{Z_{\rm eq} + jX_{22}} \tag{15}$$

As mentioned above, the $Z_{\rm eq}$ is purely resistive. Hence, the imaginary and real parts of $Z_{\rm pa}$ can be expressed as follows.

$$\begin{cases} X_{\rm pa} = X_{11} - \frac{X_{12}^2 X_{22}}{X_{22}^2 + Z_{\rm eq}^2} \\ R_{\rm pa} = \frac{X_{12}^2 Z_{\rm eq}}{X_{22}^2 + Z_{\rm eq}^2} \end{cases}. \tag{16}$$

According to (15), three degrees of freedom (X_{11}, X_{12}, and X_{22}) need to be designed when the coupling coefficient and the operating frequency are fixed. Two equations can be constructed by the target range for $X_{\rm pa}$ and $R_{\rm pa}$. Hence, it is crucial to establish an equation for obtaining the three parameters' values. Considering the high data transmission rate requirements, designing the bandwidth (BW) of IMN is necessary. In alignment with cochlear implant applications, a data rate of 1 Mbps and a BW of 6 MHz are selected. Consequently, the quality factor $Q_{\rm IMN}$ is obtained as follows:

$$Q_{\rm IMN} = \frac{f_r}{0.7{\rm BW}} = \frac{16}{0.7 \times 6} \approx 3.8. \tag{17}$$

In Fig. 10(b), a T-model impedance network is depicted, with $X_{\rm T1}$, $X_{\rm T2}$, and $X_{\rm T3}$ representing each branch's reactance at 16 MHz. The transfer relationship between the two-port network and the T-model is expressed as follows [26]:

$$\begin{cases} X_{\rm T1} = X_{11} - X_{12} \\ X_{\rm T2} = X_{22} - X_{12} \\ X_{\rm T3} = X_{12} \end{cases}. \tag{18}$$

Substituting (18) into (16), the expression of $X_{\rm pa}$ and $R_{\rm pa}$ is as

$$\begin{cases} X_{\rm pa} = X_{\rm T3} + X_{\rm T1} - \frac{X_{\rm T3}^2 (X_{\rm T3} + X_{\rm T2})}{(X_{\rm T3} + X_{\rm T2})^2 + Z_{\rm eq}^2} \\ R_{\rm pa} = \frac{X_{\rm T3}^2 Z_{\rm eq}}{(X_{\rm T3} + X_{\rm T2})^2 + Z_{\rm eq}^2} \end{cases} \tag{19}$$

According to the T-model design criteria, the range of $X_{\rm T2}$ can be determined as follows.

$$X_{\rm T2} = Z_{\rm eq} Q_{\rm IMN} = \left(\frac{k^2 \omega_r^2 L_t L_r R_L}{R_L r_r + \omega_r^2 L_r^2} + r_{\rm t} \right) Q_{\rm IMN}. \tag{20}$$

The T-model parameters can be calculated by combining (19) and (20). As mentioned above, k varies from 0.12 to 0.19. As a result, the T-model's parameters ranges are $X_{\rm T1} \in [108, 256]$, $X_{\rm T2} \in [87, 217]$, and $X_{\rm T3} \in [-121, -54]$. These parameter values indicate that the T-model comprises two inductors and one capacitor. The corresponding ranges for inductance and

capacitance are provided as

$$\begin{cases} L_{T1} \in [1.1\mu\text{H}, 2.5\mu\text{H}] \\ L_{T2} \in [0.9\mu\text{H}, 2.1\mu\text{H}] \\ C_{T3} \in [82\,\text{pF}, 185\,\text{pF}] \end{cases}. \tag{21}$$

To ensure that the impedance variation range keeps within the target region and the selected values comply with manufacturing requirements, L_{T1}, L_{T2}, and C_{T3} are designed with specific values of 1.5 μH, 1.7 μH, and 100 pF, respectively.

Based on the Class-E PA's calculation expressions provided in Section II, the PA's output voltage is shown as follows:

$$V_{pa} = 1.83 V_{dc} \exp(-0.47 \tan\varphi). \tag{22}$$

If the WPDT operates without an IMN circuit, the voltage V_{eq} is equal to V_{pa}. However, considering the influence of the IMN circuit, the voltage V_{eq} needs to be rederived, and the calculation expression is illustrated below

$$V_{eq} = \frac{V_{pa} Z_{eq} Z_{T3}}{(Z_{eq} + Z_{T2}) Z_{T3} + Z_{T1} (Z_{eq} + Z_{T2} + Z_{T3})} \tag{23}$$

where Z_{T1}, Z_{T2}, and Z_{T3} denotes the impedance of L_{T1}, L_{T2}, and C_{T3}, respectively.

According to the value of L_{T1}, L_{T2}, and C_{T3}, the expression of V_{eq} is given by the following equation:

$$V_{eq} = \frac{1.94 Z_{eq} V_{pa}}{\sqrt{Z_{eq}^2 + 122^2}}. \tag{24}$$

Based on Fig. 9(b), the coupling coefficient k is 0.19 when the coils are aligned. Substituting k into (2), the value of Z_{eq} is approximately 57.8. Hence, V_{eq} can be calculated using the following equation:

$$V_{eq} = \frac{1.94 Z_{eq} V_{pa}}{\sqrt{Z_{eq}^2 + 122^2}} \approx 1.52 V_{dc} \exp(-0.47 \tan\varphi). \tag{25}$$

The modified receiver voltage V_{r_m} is

$$V_{r\_m} = \frac{1.52 V_{dc}}{k} \sqrt{\frac{L_r}{L_t}} \exp(-0.47 \tan\varphi). \tag{26}$$

The modified V_{r_Hm} and V_{r_Lm} are as

$$\begin{cases} V_{r\_Hm} = \frac{0.89 V_{dc}}{k} \sqrt{\frac{L_r}{L_t}} \\ V_{r\_Lm} = \frac{0.89 V_{dc}}{k} \sqrt{\frac{L_r}{L_t}} \exp\left(\frac{-0.47 \omega_r L_b}{R_{pa}}\right) \end{cases}. \tag{27}$$

Class-E PA are known for their high sensitivity to fluctuations in load parameters. When its load parameters deviate from their optimal value, the system's efficiency degrades [32]. The relationship between the Class-E PA's load R_{pa} and the coupling coefficient k is given in (2). If the WPDT system operates without an IMN circuit, the R_{pa} varies from 23 to 58 Ω in the range of k from 0.12 to 0.19. Based on Section II-B, to achieve an efficiency of $\eta \geq 0.95$ and an output power range between 0.05 and 0.12 W, the Class-E PA's target impedance range, denoted as Z_{pa}, is defined as [−6, 40] for X_{pa} and [40, 67] for R_{pa}. If the IMN circuit is incorporated into the WPDT system, the calculation of R_{pa} and X_{pa} is depicted in (28), resulting in R_{pa} ranging from 41 to 67 Ω and X_{pa} ranging from -4 to 37 Ω in the range of k from 0.12 to 0.19. The R_{pa} and X_{pa} obtained by incorporating the IMN circuit satisfies the target impedance region for the Class-E PA. Hence, the addition of the IMN circuit contributes to the enhancement of robustness in WPT efficiency

$$\begin{cases} R_{pa} = \text{Re}[Z_{pa}] = \text{Re}[\frac{(R_{eq}+Z_{T2})Z_{T3}}{(R_{eq}+Z_{T2})+Z_{T3}} + Z_{T1}] \\ X_{pa} = \text{Im}[Z_{pa}] = \text{Im}[\frac{(R_{eq}+Z_{T2})Z_{T3}}{(R_{eq}+Z_{T2})+Z_{T3}} + Z_{T1}] \end{cases}. \tag{28}$$

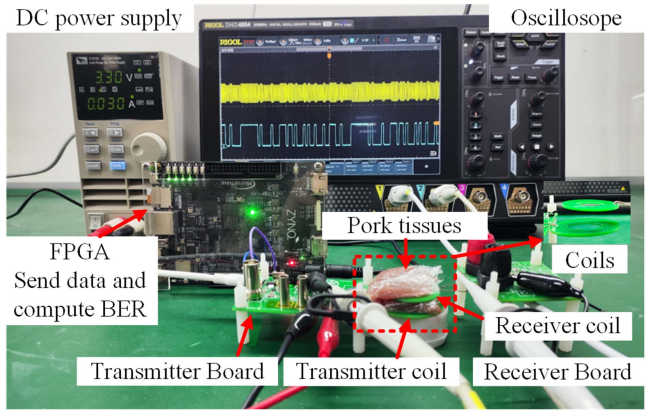

Fig. 11. Experimental platform.

TABLE III
COMPARISON OF PORK TISSUE AND HUMAN TISSUE

Tissue	εr	σ (S/m)	ρ (kg/m^3)
Pork muscle	40–50	1.0–1.5	~1040
Human muscle	50–60	1.5-2.0	~1050
Pork fat	5–8	0.03–0.08	~920
Human fat	5–10	0.05–0.1	~900

IV. EXPERIMENTAL RESULTS

The prototype of the proposed WPDT with an IMN circuit is developed for performance validation, as depicted in Fig. 11. Notably, pork tissue is employed in the experimental testing process as a surrogate for human tissue to simulate the *in vivo* environment. As shown in Table III, pork tissue exhibits physical properties—including dielectric constant (εr), conductivity (σ in S/m), and density (ρ in kg/m^3)—that closely approximate those of human tissue [35]. These similarities make pork a reliable and widely accepted substitute for experiments involving implantable devices. To ensure biomedical safety, the proposed WPDT system adopts a carrier frequency of 16 MHz, which complies with the ICNIRP and IEEE C95.1 standards for human electromagnetic exposure. This frequency remains below the 20 MHz limit specified in relevant guidelines to minimize tissue absorption and satisfy specific absorption rate constraints [36]. The design is based on the framework of commercially available cochlear implants, ensuring regulatory compatibility and safe operation in implantable applications. Besides, an FPGA board is utilized to compute the BER and generate random data signals.

TABLE IV
PARAMETERS OF THE PROTOTYPE

Parameters	Value	Parameters	Value
f_s	16 MHz	L_{T1}	1.5 μH
D	0.5	L_{T2}	1.7 μH
V_{dc}	3.3 V	C_{T3}	100 pF
C_p	30 pF	L_r	1 μH
C_o	40 pF	C_r	98 pF
L_o	3 μH	R_L	540 Ω
L_t	3 μH	R_o	1k Ω
C_t	30 pF	Coils distance	5 mm
L_a	300 nH	/	/

It is crucial to ensure that switches S_2 and S_3 exhibit low parasitic capacitance in order to prevent adverse effects on the operation of the PA. In the designed prototype, the BSS138PW from Nexperia is employed as the switching device, attributing to its advantageous characteristics such as an on-resistance of approximately 1.2 Ω and an output capacitance of 7 pF. The capacitors used in the prototype are the C0G material' MLCC series from TDK with 1% tolerances to minimize parameter errors. The selection of inductors with a self-resonant frequency higher than 300 MHz to mitigate parasitic capacitance's impact. Besides, an 800 MHz BW oscilloscope and a 500 MHz BW voltage probe are utilized to achieve highly accurate measurements. Considering the stray parameters of the circuit and components, the actual components' value is slightly adjusted. Table IV lists the prototype's parameters. Notably, the experimental measurement is divided into two parts. In one part, the *RLC* circuit depicted in Fig. 6 is utilized as the receiver's load. This setup allows for the measurement of power transmission efficiency, output power, MI, and the receiver coil's voltage. In other parts, the receiver load consists of the half-wave rectifier and a data demodulator, as illustrated in Fig. 7. The measurement includes the BER and the data demodulation waveforms.

A. Power Transmission Efficiency Robustness

Fig. 12 illustrates the performance of the WPDT circuit when the coils are aligned, where V_d and V_g represent the drain-source and gate-source voltages of S_1. In Fig. 12(a), the Class-E PA exhibits the ZVDS and ZVS features when the data signal is 1. Similarly, when the data signal is 0, it satisfies the ZVS feature, as depicted in Fig. 12(b). Experiments show that the implemented data modulation circuit meets the design requirements.

Fig. 13 depicts the receiver coil voltage waveforms for the proposed WPDT with IMN circuit. It should be noted that the misalignment distance is denoted by D_x. In Fig. 13(a), the receiver voltage waveform is presented when the coils are aligned ($D_x = 0$ mm), showcasing voltage amplitudes of 8.9 and 7.3 V for high and low data signals, respectively. Hence, the MI approaches 0.1, indicating that the result meets the design requirement. Furthermore, this operating state's output and input

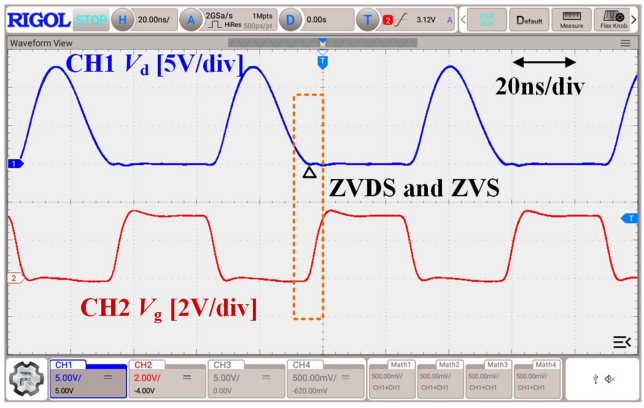

(a)

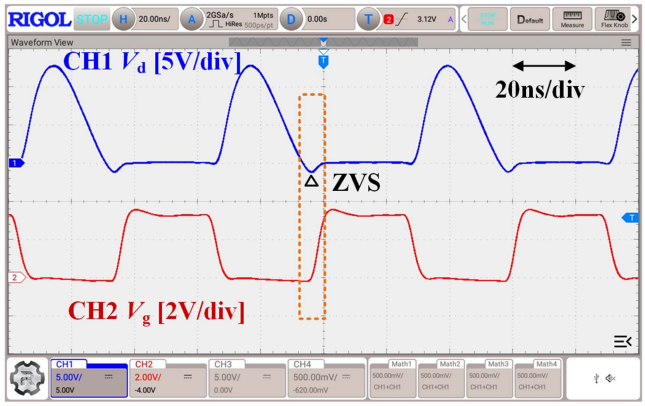

(b)

Fig. 12. Proposed WPDT circuit's experimental results. (a) V_d and V_g waveforms when the data signal is 1. (b) V_d and V_g waveforms when the data signal is 0.

TABLE V
COMPARISON RESULTS

Parameters	Calculation	Simulation	Measurement
V_{r_H}	9.9 V	9.7 V	8.9 V
V_{r_L}	8.1 V	7.9 V	7.3 V
MI	0.1	0.1	0.1

powers are 67.3 and 99 mW, respectively. The power dissipation from circuit chips is estimated to be around 10 mW. Hence, the power transmission efficiency is 61.7%.

Fig. 13(b) depicts the receiver coil voltage waveforms when $D_x = 5$ mm. The high and low data signals exhibit voltage amplitudes of 8.75 and 6.7 V, respectively, resulting in an MI value of 0.13. At this point, the power transmission efficiency measures at 58%. Moving to Fig. 13(c), as D_x increases to 10 mm, the receiver coil voltage waveform shows voltage amplitudes of 7.8 and 5.25 V for the high and low data signals. The system's efficiency is measured at 47.1% with an MI of 0.2. Furthermore, as the coil misalignment distance increases, the MI also increases.

Based on the receiver voltage's calculation expression provided in Section III, the comparing results from calculation, simulation, and measurement are outlined in Table V when the

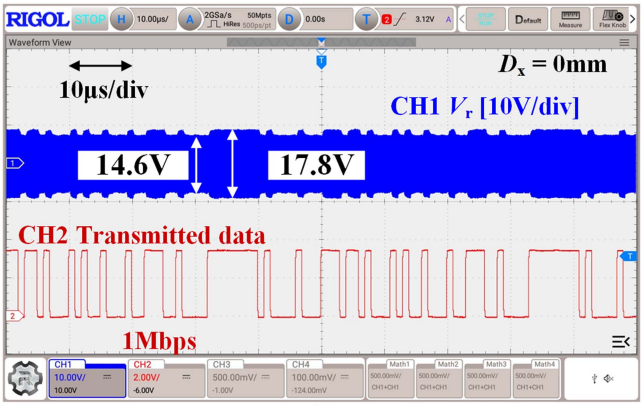

(a)

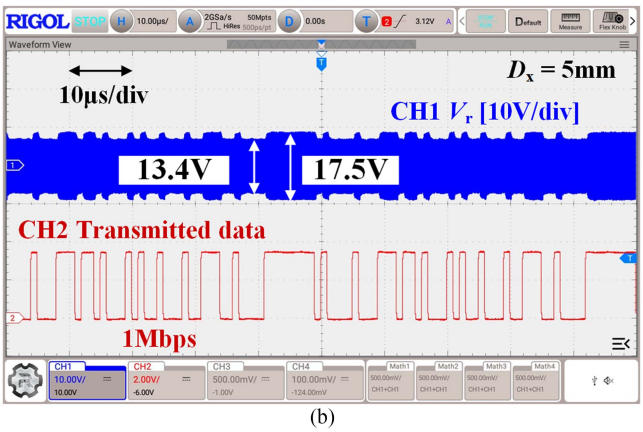

(b)

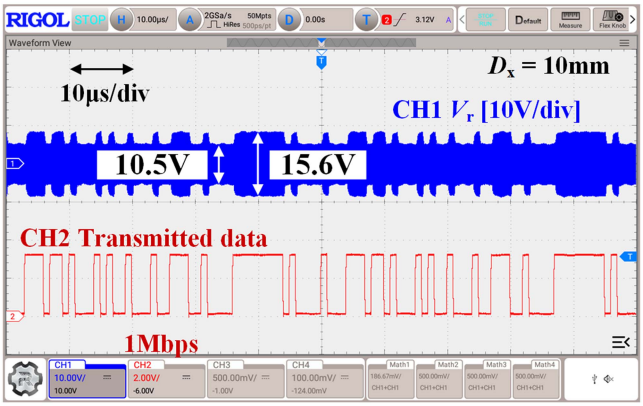

(c)

Fig. 13. Experimental waveforms of the proposed WPDT with IMN circuit when the data rate is 1 Mbps. (a) $D_x = 0$ mm. (b) $D_x = 5$ mm. (c) $D_x = 10$ mm.

coils are aligned. It is evident that the simulation results closely approximate the calculation results. However, there is some error between the measurement results and calculation results. These disparities can be attributed to the circuit's parasitic parameters, reducing the receiver coil's voltage. In addition, the value of MI is the same for calculation, simulation, and measurement, demonstrating the proposed calculation method's effectiveness.

Fig. 14 presents a comparative analysis of experimental results for the proposed WPDT with and without an IMN circuit, considering output voltage RMS and system efficiency. Notably, a misalignment weight factor is incorporated in Fig. 14 to quantify the severity of misalignment between coils. This factor

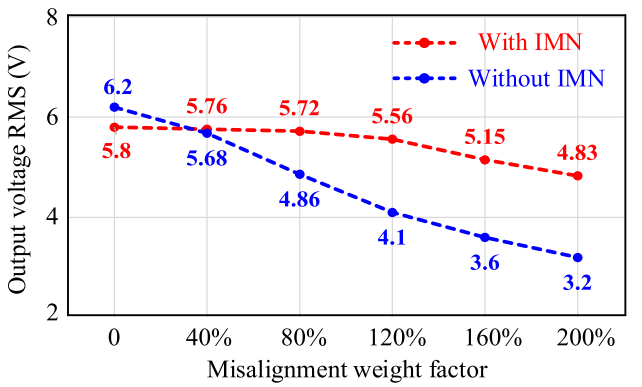

(a)

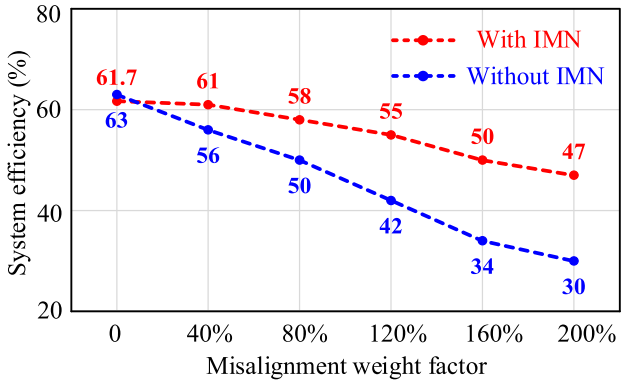

(b)

Fig. 14. Performance comparison under different misalignment weight factors. (a) Receiver coil's RMS voltage with different misalignment weight factors. (b) System efficiency with different misalignment weight factors.

is determined by the ratio of the misalignment distance to the vertical distance between the transmission and receiver coils. For misalignment distances ranging from 0 to 10 mm and a fixed vertical distance of 5 mm between the coils, the misalignment weight factor varies from 0% to 200%. As the misalignment distance increases, the weight factor's value correspondingly rises.

In Fig. 14(a), the RMS voltage of the receiver coil is depicted for various misalignment weight factors. The red and blue curves illustrate the trends in output voltage RMS for the WPDT with and without the IMN circuit. Notably, for the proposed WPDT circuit with an IMN circuit, the output voltage exhibits a modest variation from 5.8 to 4.83 V across the range of misalignment weight factors, with a particularly slight fluctuation of less than 0.3 V within the 0% to 120% range. In contrast, the WPDT without the IMN circuit experiences a more substantial voltage change, ranging from 6.2 to 3.2 V. Consequently, the proposed WPDT with an IMN circuit demonstrates enhanced robustness in maintaining output voltage stability against misalignment.

The variation trends in power transmission efficiency with different misalignment factors are depicted in Fig. 14(b). For the proposed WPDT with the IMN circuit, the system efficiency ranges from 61.7% to 47% across the misalignment weight factors, showcasing a 17% improvement at the highest 200%

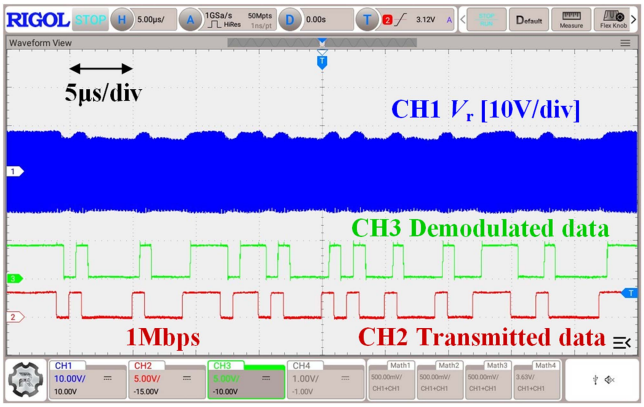

Fig. 15. Data demodulation waveform with a data rate of 1 Mbps when coils are aligned.

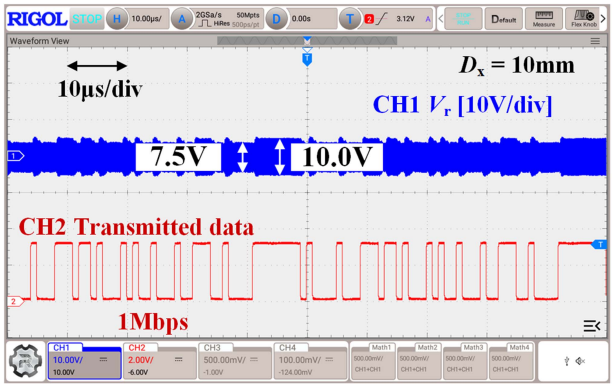

Fig. 16. Experimental waveforms of the WPDT without IMN circuit when $D_x = 10$ mm.

misalignment weight factor. In contrast, the WPDT without the IMN circuit experiences a more significant efficiency drop, ranging from 63% to 30% within the same interval. It is evident that adopting the WPDT with the IMN circuit enhances power transmission efficiency, especially under severe misalignment conditions. The efficiency reduction for misalignment weight factors ranging from 0% to 200% is notable in the WPDT without an IMN, reaching up to 33%. Hence, the IMN circuit significantly improves power transmission efficiency in misalignment scenarios.

B. Data Transmission Robustness

The BER serves as a critical metric for evaluating the reliability and robustness of data transmission. A lower BER signifies enhanced reliability in data transmission. Hence, to assess the bit error rate, several million random bits are transmitted from the FPGA and subsequently received by the FPGA via the data demodulation circuit. After performing calculations within the FPGA, it is calculated that the BER is less than 10^{-6} for a 1 Mbps data rate. Fig. 15 displays the experimental waveform with a 1 Mbps data rate when the coils are aligned, including the transmitted data, demodulated data, and the receiver coil voltage. Notably, the demodulated data waveform closely matches the transmitted data waveform. As mentioned above, the MI increases as the coil misalignment distance increases. Therefore, the BER will be below 10^{-6} when the coil misalignment ranges from 0 to 10 mm, contributing to enhanced robustness in data transmission.

In contrast, the WPDT without IMN circuit exhibits an approximate MI measurement of 0.14 in case of 10 mm coil misalignment, as illustrated in Fig. 16. Conversely, the MI of the proposed WPDT with IMN circuit is measured to be 0.2 under the same operating condition, as shown in Fig. 13(c). Hence, the experimental result indicates that the proposed circuit effectively improves data transmission robustness in misalignment scenarios.

Overall, it can be concluded that the proposed WPDT with an IMN circuit for IMDs improves the power transmission efficiency's robustness and ensures the data transmission's reliability in cases of coil misalignment.

TABLE VI
COMPARISON WITH PREVIOUS WORKS

References	2018 [37]	2018 [7]	2018 [32]	2020 [38]	This work
Modulation	PSK	FSK	ASK	OOK	ASK
Carrier frequency (MHz)	13.56	2/4	10	2.5	16
Data rate (Mbps)	0.1	1	1	0.625	1
Bit error rate	/	10^{-5}	10^{-5}	10^{-5}	10^{-6}
Coil distance (mm)	/	6	6	10	5
PDL (mW)	54	126	24	80	62
PTE (%)	48	25	42	20	61.7
Coil misalignment distance (mm)	0	0	0	0	0–10
PTE range (%)	/	/	/	/	61.7–47

C. WPDT Implementation Strategies Comparisons

The proposed WPDT circuit has been evaluated against existing literature, with its unique attributes delineated in Table VI. The comparison results demonstrate that the WPDT developed in this study exhibits superior performance, particularly in scenarios involving coil misalignment. Furthermore, the proposed WPDT circuit is also characterized by its high power transmission efficiency.

The studies listed in Table VI are dedicated to the exploration of diverse data modulation strategies and circuit designs, with a primary focus on optimizing transmission efficiency and rate within a specified coil distance. Despite the potential impact of coil misalignment on system transmission performance, these investigations have not thoroughly considered the degradation in potential transmission efficiency and data transmission rate characteristics that may arise from such misalignments. In this article, we aim to fill this research gap by specifically addressing the challenges associated with the degradation of power transmission efficiency and data transmission rate for IMDs when coil misalignment. Given the distinct nature of these challenges, it is imperative to recognize that a direct comparison of the

studies listed in Table VI may not be entirely fair, as they do not uniformly account for the complexities introduced by coil misalignment. This article aims to provide a comprehensive analysis of the effects of coil misalignment on IMD performance, offering a more nuanced perspective that can inform the design of robust and reliable systems for medical applications.

V. Conclusion

This study presents an innovative WPDT circuit, incorporating an impedance-matching network to address the robustness of coil misalignment. A comprehensive exploration is presented, which includes the implementation of the data modulation and IMN circuit and the calculation of the theoretical design methodology. This research also contributes by identifying and considering the constraint condition on data transmission rates to design the IMN, which ensures a high data transmission rate in IMDs. Experimental results demonstrate a 17% enhancement in the power transmission efficiency and minimal output voltage fluctuation (less than 1 V) compared to without an IMN circuit when the coil misalignment distance reaches 10 mm (i.e., 200% misalignment weight factor). The bit error bit, which evaluates the data transmission reliability, is less than 10^{-6} in cases of 1 Mbps data rate with a MI of 10%. Consequently, the proposed circuit can effectively enhance the robustness when the coils are misaligned in terms of power transmission efficiency and data transmission reliability.

The current study focuses on a low-power WPDT system in IMDs utilizing loosely coupled magnetic links with unidirectional data transmission. While effective for basic telemetry, many real-world applications, such as neural recording or bidirectional communication in implantable medical systems, require half-duplex or full-duplex data exchange. This presents a significant challenge: how to achieve high-speed bidirectional data transfer over a single magnetic coupling channel, while simultaneously maintaining high-efficiency power delivery. To address this dual-objective constraint, future work will investigate the integration of advanced modulation techniques, signal multiplexing, and timing control strategies. In addition, the system's robustness under misalignment can be further improved by incorporating adaptive impedance matching algorithms or real-time auto-tuning networks, enabling more reliable performance under dynamic in vivo conditions.

References

[1] F. Henry, M. Glavin, and E. Jones, "Noise reduction in Cochlear implant signal processing: A review and recent developments," *IEEE Rev. Biomed. Eng.*, vol. 16, pp. 319–331, 2023.

[2] Y. Rezaeiyan, M. Zamani, O. Shoaei, and W. A. Serdijn, "Mixed-signal IC with pulse width modulation wireless telemetry for implantable cardiac pacemakers in 0.18-μm CMOS," *IEEE Trans. Biomed. Circuits Syst.*, vol. 12, no. 3, pp. 589–600, Jun. 2018.

[3] A. Trigui, S. Hached, A. C. Ammari, Y. Savaria, and M. Sawan, "Maximizing data transmission rate for implantable devices over a single inductive link: Methodological review," *IEEE Rev. Biomed. Eng.*, vol. 12, pp. 72–87, Oct. 2018.

[4] K. Dehghan, O. Shoaei, and S. J. Ashtiani, "A class-E power and data transmitter with improved data rate to carrier frequency ratio for medical implants," *IEEE Trans. Circuits Syst. II Exp. Briefs*, vol. 69, no. 6, pp. 2692–2696, Jun. 2022.

[5] M. Liu, H. Zhang, Y. Shao, J. Song, and C. Ma, "High-performance megahertz wireless power transfer: Topologies, modeling, and design," *IEEE Ind. Electron. Mag.*, vol. 15, no. 1, pp. 28–42, Mar. 2021.

[6] M. Fu, H. Yin, M. Liu, and C. Ma, "Loading and power control for a high-efficiency class E PA-driven megahertz WPT system," *IEEE Trans. Power Electron.*, vol. 63, no. 11, pp. 6867–6876, Nov. 2016.

[7] M. M. Ahmadi and S. Ghandi, "A class-E power amplifier with wideband FSK modulation for inductive power and data transmission to medical implants," *IEEE Sensors J.*, vol. 18, no. 17, pp. 7242–7252, Sep. 2018.

[8] W. Huang, K. Shan Zheng, X. Liu, X. Wang, Y. Hou, and Y. Liu, "Simultaneous high-efficiency power delivery and energy-efficient forward data transmission over single inductive link," *IEEE Access*, vol. 11, pp. 76793–76803, 2023.

[9] Y. Chen, Y. Liu, Y. Li, G. Wang, and M. Chen, "An energy-efficient ASK demodulator robust to power-carrier-interference for inductive power and data telemetry," *IEEE Trans. Biomed. Circuits Syst.*, vol. 16, no. 1, pp. 108–118, Feb. 2022.

[10] S. Roy, A. N. M. W. Azad, S. Baidya, M. K. Alam, and F. Khan, "Powering solutions for biomedical sensors and implants inside the Human body: A comprehensive review on energy harvesting units, energy storage, and wireless power transfer techniques," *IEEE Trans. Power Electron.*, vol. 37, no. 10, pp. 12237–12263, Oct. 2022.

[11] D. Ahn and M. Ghovanloo, "Optimal design of wireless power transmission links for millimeter-sized biomedical implants," *IEEE Trans. Biomed. Circuits Syst.*, vol. 10, no. 1, pp. 125–137, Feb. 2016.

[12] M. J. Karimi, A. Schmid, and C. Dehollain, "Wireless power and data transmission for implanted devices via inductive links: A systematic review," *IEEE Sensors J.*, vol. 21, no. 6, pp. 7145–7161, Mar. 2021.

[13] J. Feng, G. Wei, J. Cui, J. Zhang, F. Chen, and C. Zhu, "A high-misalignment-tolerant and extensive vertical adaptation combined simultaneous transmission of power and data for WPT system," *IEEE J. Emerg. Sel. Topics Power Electron.*, vol. 11, no. 6, pp. 6138–6149, Dec. 2023.

[14] D. Liu, H. Hu, and S. V. Georgakopoulos, "Misalignment sensitivity of strongly coupled wireless power transfer systems," *IEEE Trans. Power Electron.*, vol. 32, no. 7, pp. 5509–5519, Jul. 2017.

[15] A. Basir, I. A. Shah, and H. Yoo, "Sphere-shaped receiver coil for misalignment-resilient wireless power transfer systems for implantable devices," *IEEE Trans. Antennas Propag.*, vol. 70, no. 9, pp. 8368–8378, Sep. 2022.

[16] S. Y. Choi, J. Huh, W. Y. Lee, and C. T. Rim, "Asymmetric coil sets for wireless stationary EV chargers with large lateral tolerance by dominant field analysis," *IEEE Trans. Power Electron.*, vol. 29, no. 12, pp. 6406–6420, Dec. 2014.

[17] S. Y. Choi, S. Y. Jeong, E. S. Lee, B. W. Gu, S. W. Lee, and C. T. Rim, "Generalized models on self-decoupled dual pick-up coils for large lateral tolerance," *IEEE Trans. Power Electron.*, vol. 30, no. 11, pp. 6434–6445, Nov. 2015.

[18] G. Ke, Q. Chen, W. Gao, S.-C. Wong, C. K. Tse, and Z. Zhang, "Research on IPT resonant converters with high misalignment tolerance using multicoil receiver set," *IEEE Trans. Power Electron.*, vol. 35, no. 4, pp. 3697–3712, Apr. 2020.

[19] T.-C. Yu, W.-H. Huang, and C.-L. Yang, "Design of dual frequency mixed coupling coils of wireless power and data transfer to enhance lateral and angular misalignment tolerance," *IEEE J. Electromagn. RF Microw. Med. Biol.*, vol. 3, no. 3, pp. 216–223, Sep. 2019.

[20] D. Wu, R. Mai, S. Zhao, Z. He, and F. Peng, "A self-oscillating controller based on pulse density modulator in wireless power transfer," in *Proc. IEEE Energy Convers. Congr. Expo.*, 2019, pp. 2125–2128.

[21] Z. Wei, B. Zhang, S. Lin, and C. Wang, "A self-oscillation WPT system with high misalignment tolerance," *IEEE Trans. Power Electron.*, vol. 39, no. 1, pp. 1870–1887, Jan. 2024.

[22] D. Bui, G. Wang, L. Zhao, and A. P. Hu, "A bidirectional autonomous high-frequency wireless power transfer system with constant voltage output against load and coupling variations," *IEEE J. Emerg. Sel. Topics Power Electron.*, vol. 11, no. 6, pp. 6159–6167, Dec. 2023.

[23] Y. Lim, H. Tang, S. Lim, and J. Park, "An adaptive impedance-matching network based on a novel capacitor matrix for wireless power transfer," *IEEE Trans. Power Electron.*, vol. 29, no. 8, pp. 4403–4413, Aug. 2014.

[24] W. Zhong and S. Y. R. Hui, "Auxiliary circuits for power flow control in multifrequency wireless power transfer systems with multiple receivers," *IEEE Trans. Power Electron.*, vol. 30, no. 10, pp. 5902–5910, Oct. 2015.

[25] D. Ahn and S. Hong, "A transmitter or a receiver consisting of two strongly coupled resonators for enhanced resonant coupling in wireless power transfer," *IEEE Trans. Ind. Electron.*, vol. 61, no. 3, pp. 1193–1203, Mar. 2014.

[26] E. Chung and J.-I. Ha, "Impedance matching network design for 6.78 MHz wireless power transfer system with constant power characteristics against misalignment," *IEEE Trans. Power Electron.*, vol. 39, no. 1, pp. 1788–1801, Jan. 2024.
[27] Y. Shao, H. Zhang, M. Liu, and C. Ma, "Explicit design of impedance matching networks for robust MHz WPT systems with different features," *IEEE Trans. Power Electron.*, vol. 37, no. 9, pp. 11382–11393, Sep. 2022.
[28] M. Liu, S. Liu, and C. Ma, "A high-efficiency/output power and low-noise megahertz wireless power transfer system over a wide range of mutual inductance," *IEEE Trans. Microw. Theory Tech.*, vol. 65, no. 11, pp. 4317–4325, 2017.
[29] X. Zhang, J. Li, and X. Tong, "A unique design approach of double-sided LCC compensated IPT system for misalignment-tolerant characteristic," *IEEE Trans. Power Electron.*, vol. 38, no. 1, pp. 1288–1300, Jan. 2023.
[30] F. Raab, "Idealized operation of the class E tuned power amplifier," *IEEE Trans. Circuits Syst.*, vol. CAS-24, no. 12, pp. 725–735, Dec. 1977.
[31] M. M. Ahmadi, S. Pezeshkpour, and Z. Kabirkhoo, "A high-efficiency ASK-modulated class-E power and data transmitter for medical implants," *IEEE Trans. Power Electron.*, vol. 37, no. 1, pp. 1090–1101, Jan. 2022.
[32] M. Lotfi Navaii, H. Sadjedi, and A. Sarrafzadeh, "Efficient ASK data and power transmission by the class-E with a switchable tuned network," *IEEE Trans. Circuits Syst. I Reg. Papers*, vol. 65, no. 10, pp. 3255–3266, Oct. 2018.
[33] J. Olivo, S. Carrara, and G. De Micheli, "A study of multi-layer spiral inductors for remote powering of implantable sensors," *IEEE Trans. Biomed. Circuits Syst.*, vol. 7, no. 4, pp. 536–547, Aug. 2013.
[34] Y. Palagani, K. Mohanarangam, J. H. Shim, and J. R. Choi, "Wireless power transfer analysis of circular and spherical coils under misalignment conditions for biomedical implants," *Biosensors Bioelectron.*, vol. 141, Sep. 2019, Art. no. 111283.
[35] C. Gabriel, S. Gabriel, and Y. E. Corthout, "The dielectric properties of biological tissues: I. Literature survey[J]," *Phys. Med. Biol.*, vol. 41, no. 11, 1996, Art. no. 2231.
[36] Y. Jia et al., "Position and orientation insensitive wireless power transmission for EnerCage-homecage system," *IEEE Trans. Biomed. Eng.*, vol. 64, no. 10, pp. 2439–2449, Oct. 2017.
[37] C.-H. Cheng et al., "A fully integrated 16-channel closed-loop neural-prosthetic CMOS SoC with wireless power and bidirectional data telemetry for real-time efficient Human epileptic seizure control," *IEEE J. Solid-State Circuits*, vol. 53, no. 11, pp. 3314–3326, Nov. 2018.
[38] M. M. Ahmadi and M. Sarbandi-Farahani, "A Class-E power and data transmitter with on–off keying data modulation for wireless power and data transmission to medical implants," *Circuits, Syst., Signal Process*, vol. 39, pp. 4174–4186, 2020.

Haoqi Zhu (Member, IEEE) received the M.S. degree in control science and engineering from Hangzhou Dianzi University, Hangzhou, China, in 2019, and the Ph.D. degree in electrical engineering from Zhejiang University, Hangzhou, China, in 2024.

He is currently a postdoctoral researcher with Zhejiang University. His current research interests include modeling and analysis of power electronics, controlling and applications, high-frequency power converters with wide bandgap devices, wireless power and data transmission, grid connection of renewable energy, grid-forming equipment, and energy storage systems.

Xu Wu (Member, IEEE) was born in Yancheng, Jiangsu Province, China, in 1992. He received the B.S. degree in electrical engineering and master's degree in automation engineering from Nanjing University of Posts and Telecommunications, Nanjing, China, in 2015 and 2018, respectively, and the Ph.D. degree in electrical engineering from Nanjing University of Aeronautics and Astronautics (NUAA), Nanjing, China, in 2022.

From 2022 to 2024, he worked as a postdoctoral researcher with Zhejiang University, Hangzhou, China, focusing on the gate drive and short-circuit protection of medium voltage 3.3 kV SiC MOSFET module. He is currently a Senior R&D Engineer with State Grid Electric Power Research Institute/NARI Group Corporation, Nanjing, China. His research interests include power electronics, motor drive, grid-forming equipment, and energy storage systems.

Feng Xiong was born in Huangshi, Hubei Province, China, in 2004. He is currently working toward the B.S. degree in electronic information engineering with the College of Physics and Electronic Science, Hubei Normal University, Huangshi, China.

His current research interests include wireless power and data transmission, electronic information engineering, and power electronics.

Mustafa Tahir (Member, IEEE) received the B.Sc. degree in electrical engineering from the University of Engineering and Technology Lahore, Lahore, Pakistan, in 2015, the M.S. degree in electrical engineering from the Nanjing University of Aeronautics and Astronautics, Nanjing, China, in 2020, and the Ph.D. degree in electrical engineering from Zhejiang University, Hangzhou, China, in 2024.

He is currently a postdoctoral researcher with Zhejiang University. His current research interests include electric vehicle charging solutions, renewable energy systems, hydrogen energy systems, power converters, and wide-bandgap devices applications.

Dr. Mustafa is the recipient of the Excellent Paper Award of the IACGN in 2019, the Excellent Presenter Award of CEES 2022, the University Scientist Award by Infineon at PCIM 2022, and the Excellent Researcher Award by Zhejiang University in 2023. He actively contributes as a peer reviewer for over 20 reputable international journals, including various IEEE Transactions. He is a Lifetime Member as well as a Registered Engineer with the Pakistan Engineering Council.